J. Fluid Mech. (1996), vol. 312, pp. 279–298



# Torsional flow: elastic instability in a finite domain

By AARON AVAGLIANO AND NHAN PHAN-THIEN
Department of Mechanical and Mechatronic Engineering, The University of Sydney, NSW 2006, Australia

(Received 10 April 1995 and in revised form 14 November 1995)

A rotational shear flow is examined in the parallel plate geometry for the Oldroyd-B fluid. The Stokes solution is found to have eigenfunctions in an unbounded radial domain while it is unique for general boundary conditions in a finite radial domain. Critical conditions for the onset of an axisymmetric secondary flow are determined for the viscoelastic fluid, and we show that there is an almost linear relationship between the aspect ratio of the plates and the critical Deborah number for this model, especially at small values of the aspect ratio. The form of the initial secondary flow is also in agreement with experimental results obtained for a Boger fluid.

## 1. Introduction

Rotational flow instabilities were first observed in parallel plate rheometers over a decade ago by Jackson, Walters & Williams (1984), who observed antithixotropic behaviour in a Boger fluid. This instability had been predicted by Phan-Thien (1983) in a theoretical analysis of the Oldroyd-B model of a viscoelastic fluid. Assuming that the parallel plates were of infinite extent, Phan-Thien was able to show that an elastic instability occurred in the viscometric base solution at a critical value of the rotation rate. The unbounded radial domain permitted the use of Lie group symmetries to reduce the order of the problem, and allowed an analytic result to be obtained. However, the unbounded radial domain excluded the possibility of examining the effect of varying the gap width of the plates on the critical rotation rate. This was achieved experimentally by Magda & Larson (1988), who examined the effect of varying gap width on the critical rim shear rate $\dot{\gamma}$, and concluded that $\dot{\gamma}$ was approximately inversely proportional to the gap width. The flow visualisation experiments of McKinley *et al.* (1991) showed conclusively that the apparent shear thickening was not due to a build up in the structure of the fluid, but rather to the development of a secondary flow. This flow was initially axisymmetric with roll cells forming at the centreline travelling outwards, and those forming at the outer edge travelling in towards the centre. The disturbance quickly became non-axisymmetric with the formation of spiral vortices, and finally developed into fully nonlinear flow. They also showed that the amplitude of the initial disturbances *increased exponentially in time*, indicating that a linear stability analysis is an effective method of determining critical points on the solution curves.

In dealing with a theoretical prediction of the instability, all of the current work (with the exception of Olagunju 1994) utilizes semi-infinite geometry to obtain solutions. Olagunju used a regular perturbation scheme to study secondary inertial flows that occur for fluids with arbitrary relaxation times. He investigated these flows using

a geometry in which the fluid was held in by surface tension. Beyond a critical rotation rate the scheme broke down, indicating either that a critical rotation rate had been reached, or that the scheme was no longer valid beyond this rate.

Öztekin & Brown (1993) examined the stability of the base viscometric flow to radially localized disturbances for the Oldroyd-B model in the semi-infinite domain, in an attempt to emulate the experimental results of McKinley *et al.* (1991) numerically. In solving the resulting system of ordinary differential equations obtained from their three-dimensional analysis, they determined that at a critical value of the dimensionless radius (a function of rotation rate) elastic instability produced a secondary flow, with the most dangerous mode being non-axisymmetric. Axisymmetric disturbances were only slightly less unstable. For a suitable choice of the single relaxation time of the Oldroyd-B model, their analysis agreed quantitatively with the experiments of McKinley *et al.* (1991).

This analysis was extended by Byars *et al.* (1994), who conducted a series of experiments using two polyisobutylene/polybutene Boger fluids. The first was the same as that used by McKinley *et al.* (1991) and the second was a more dilute solution with a smaller elastic contribution to the total viscosity. They were able to extend the analysis of Öztekin & Brown (1993) using the Chilcott–Rallison model. In this model the polyisobutylene molecules are treated as a dilute solution of non-interacting dumbbells, the end beads of which are connected by a spring of finite extensibility. This results in a nonlinear constitutive equation that allows for the effect of shear thinning of the first normal stress difference. Using the fact that the stress ratio (the local ratio of the first normal stress difference to the shear stress) increases linearly outward from the centre of the discs in the radial direction for the Oldroyd-B model, while approaching a limiting constant for the Chilcott–Rallison model, they showed that the instability occurring at the critical radius ($R_1$) of the Öztekin & Brown analysis was then damped by shear thinning and disappeared beyond a second critical radius ($R_2$). The advantage of this is that the boundary conditions at the outer edge, and the symmetry conditions at the centreline, can be neglected. Once again, non-axisymmetric disturbances were the most unstable, and this was borne out by the accompanying experiments. The resulting secondary flow was well described by the analysis, except that the critical radii calculated were smaller than those obtained experimentally.

The analyses of Olagunju and Byars *et al.* (1994) indicate that the presence of the free surface is not of extreme importance, since it is perturbed by only a small amount due to secondary flows, so that the significant factor in the observed difference between the eigenfunctions of Phan-Thien's analysis, and the observed disturbance field of McKinley *et al.* (1991), is due to the presence of an outer boundary. We assume discs of finite extent, with the fluid being held between the plates by a rigid frictionless outer bounding shell. This assumption seems sufficient to achieve a far more accurate correspondence between theory and experiment. The simplifying assumptions (e.g. symmetry reduction, normal mode analysis), can no longer be applied, and we must solve a two-dimensional problem for the case of axisymmetric disturbances. We restrict ourselves to axisymmetric instability as a first step to a more physically realistic model, so that the results compare most closely with the original experiments of McKinley *et al.* (1991).

Most of the current work on rotational instabilities has dealt experimentally with Boger fluids, and theoretically with the Oldroyd-B model, one of the simplest constitutive equations used to describe the behaviour of viscoelastic fluids (a thorough account is available in the review article of Larson 1992). However, available evidence

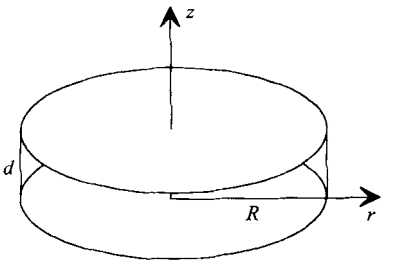


FIGURE 1. Flow geometry

suggests that the Oldroyd-B model, while able to predict the form of the secondary flow, may not be sufficient to quantitatively predict the critical rotation rate for the onset of the disturbance in these Boger fluids. The single relaxation time of the model is generally determined by the zero-shear-rate first normal stress coefficient, while some Boger fluids have been shown to exhibit a certain amount of shear thinning of the first normal stress coefficient (McKinley *et al.* 1991). We show that the correlation between theory and experiment is greatly improved when the relaxation time is chosen to reflect the shear rate at which the instability sets in.

The bounded case also cannot readily be reduced to the unbounded case in a limiting sense. This is evident in the preliminary results obtained for both cases on the uniqueness of the torsional flow solution. We show that the simplification of assuming an unbounded flow leads to a loss of uniqueness of the torsional flow solution in the case of Stokes' flow, while the solution for bounded flow is unique. Hence, the unbounded case cannot be considered as a limiting process of the finite geometry.

## 2. Governing equations and flow geometry

To model the parallel plate rheometer we assume a geometrical construction of two circular discs with a common axis through their centres. The discs are a distance $d$ apart and have a common radius (see figure 1). Two radial lengths are considered. In the first we consider the semi-infinite geometry in which the radial coordinate is unbounded, while in the second we assume that the fluid is enclosed at $r_* = R$ by a frictionless bounding shell (one that cannot sustain a shear stress). The top plate is set spinning at an angular velocity $\omega$, while the bottom plate remains stationary.

The governing field equations are

$$\rho \frac{\mathrm{D}\boldsymbol{v}_*}{\mathrm{D}t} = -\nabla_* P_* + \nabla_* \cdot \boldsymbol{S}_*, \qquad \nabla_* \cdot \boldsymbol{v}_* = 0, \tag{1}$$

where $\rho$ is the fluid density, $\frac{\mathrm{D}}{\mathrm{D}t}$ the material time derivative, $P_*$ the pressure field, and $\boldsymbol{S}_*$ and $\mathbf{v}_*$ the extra stress and the velocity fields respectively. $\boldsymbol{S}_*$ is given by $\mathbf{S}_* = \tau_{s*} + \tau_{p*}$, the solvent and polymeric contributions to the stress. The solvent contribution is simply the Newtonian stress term $\tau_{s*} = 2\eta_s \boldsymbol{D}_*$, while for the polymeric stress, we consider the upper convected Maxwell model,

$$\tau_{p*} + \lambda \left\{ \frac{\partial \tau_{p*}}{\partial t} + \boldsymbol{u} \cdot \nabla \tau_{p*} - \boldsymbol{L}_* \tau_{p*} - \tau_{p*} \boldsymbol{L}_*^{\,T} \right\} = 2\eta_p \boldsymbol{D}_*. \tag{2}$$

The constitutive model collectively is known as the Oldroyd fluid B. Here we have $\lambda$ as the sole relaxation time, $\boldsymbol{L}_* = (\nabla_* \boldsymbol{v}_*)^T$ is the velocity gradient tensor, with $\boldsymbol{D}_*$ as its symmetric part, and the total viscosity $\eta = \eta_s + \eta_p$. We focus on the Oldroyd-

B model, since most of the experimental work (Magda & Larson 1988; McKinley *et al.* 1991; Byars *et al.* 1994) was done using Boger fluids, which are supposedly amenable to this simpler type of constitutive equation, having only two material parameters (actually three parameters, but only two dimensionless groups remain after normalization). The model predicts constant viscosity $\eta$ and a constant first normal stress coefficient $\Psi_1$. However, experimental evidence from several investigators shows significant differences in the rheological behaviour of different Boger fluids. In Larson, Shaqfeh & Muller (1990), the 1000 p.p.m. Boger fluid examined shows little shear thinning over the range of shear rates covered. The current investigation compares numerical results with experimental results obtained by McKinley *et al.* (1991) for a 3100 p.p.m. Boger fluid. While maintaining a constant viscosity over the relevant range of shear rates, $\Psi_1$ exhibits a moderate amount of shear thinning (to approximately one quarter of its initial value).

For cylindrical polar coordinates $(r_*, \theta, z_*)$ in the finite regime we non-dimensionalize as

$$\left.\begin{aligned} &z = \frac{z_*}{d}, \quad r = \frac{r_*}{R}, \quad t = \omega t_*, \quad v_\theta = \frac{v_{\theta *}}{\omega R}, \quad v_r = \frac{v_{r*}}{\omega R}, \quad v_z = \frac{v_{z*}}{\omega d}, \\ &De = \lambda\omega, \quad \varepsilon = \frac{d}{R}, \quad Re = \frac{\rho\omega d R}{\eta}, \quad \beta = \frac{\eta_p}{\eta}, \\ &P = \varepsilon^2 \frac{P_*}{\eta\omega}, \quad \tau_{zz} = \frac{\tau_{pzz*}}{\eta\omega}, \quad \tau_{rz} = \varepsilon \frac{\tau_{prz*}}{\eta\omega}, \quad \tau_{rr} = \varepsilon^2 \frac{\tau_{prr*}}{\eta\omega}, \\ &\tau_{\theta\theta} = \varepsilon^2 \frac{\tau_{p\theta\theta*}}{\eta\omega}, \quad \tau_{r\theta} = \varepsilon^2 \frac{\tau_{pr\theta*}}{\eta\omega}, \quad \tau_{\theta z} = \varepsilon \frac{\tau_{p\theta z*}}{\eta\omega}. \end{aligned}\right\} \tag{3}$$

*De* is the Deborah number, being the ratio of fluid relaxation time to the characteristic time scale, *Re* is the Reynolds number, $\beta$ is the retardation parameter ($\beta = 0$ gives the Newtonian case, while $\beta = 1$ gives the Maxwell model), and $\varepsilon$ is the aspect ratio of the discs.

To non-dimensionalize in the semi-infinite regime the radial coordinate, and velocities, must be scaled by *d*. The non-dimensional groups are scaled accordingly and the equations of state and boundary conditions (except at $r_* = R$) for this geometry are recovered by setting $\varepsilon = 1$.

### 2.1. *Boundary conditions*

The no-slip boundary conditions on the upper and lower plates require that

$$\left.\begin{aligned} &v_r = v_z = v_\theta = 0 \quad \text{at} \quad z = 0, \\ &v_r = v_z = 0, \quad v_\theta = r \quad \text{at} \quad z = 1. \end{aligned}\right\} \tag{4}$$

Symmetry conditions at the centreline dictate a zero radial and azimuthal velocity, as well as zero shear stress there, i.e.

$$v_r = v_\theta = 0, \quad \tau_{r\theta} = \tau_{rz} = 0 \quad \text{at} \quad r = 0. \tag{5}$$

Boundary conditions are not generally imposed at infinity, which is shown later in the text to lead to loss of uniqueness of the Newtonian solution to another physically realistic solution.

In the finite geometry, we have no flow through boundary ($\boldsymbol{v} \cdot \boldsymbol{n} = 0$, $\boldsymbol{n} = (1,0,0)$), and the traction only acts in a direction normal to the boundary ($\boldsymbol{\tau} \cdot \boldsymbol{n} - \boldsymbol{\tau} : \boldsymbol{nnn} = \boldsymbol{0}$), i.e.

$$v_r = 0, \quad \tau_{r\theta} = \tau_{rz} = 0 \quad \text{at} \quad r = 1. \tag{6}$$

## 3. Solutions for Newtonian and viscoelastic flows

In the absence of inertia, the steady torsional flow solution ($\boldsymbol{v} = (0, rz, 0)$) is valid for the Oldroyd-B model, in the unbounded case, since the flow is controllable. What is not generally known is that it is also valid for the bounded case, as it satisfies the boundary conditions exactly at $r = 1$. The governing equations may be written as

$$-\frac{\partial P}{\partial r} + \frac{1}{r}\frac{\partial}{\partial r}(r\tau_{rr}) + \frac{\partial \tau_{rz}}{\partial z} - \frac{\tau_{\theta\theta}}{r} + (1-\beta)\left[\varepsilon^2 \frac{\partial}{\partial r}\left(\frac{1}{r}\frac{\partial}{\partial r}(rv_r)\right) + \frac{\partial^2 v_r}{\partial z^2}\right] = 0, \tag{7}$$

$$\frac{1}{r^2}\frac{\partial}{\partial r}(r^2\tau_{r\theta}) + \frac{\partial \tau_{\theta z}}{\partial z} + (1-\beta)\left[\varepsilon^2 \frac{\partial}{\partial r}\left(\frac{1}{r}\frac{\partial}{\partial r}(rv_\theta)\right) + \frac{\partial^2 v_\theta}{\partial z^2}\right] = 0, \tag{8}$$

$$-\frac{\partial P}{\partial z} + \varepsilon^2\left\{\frac{1}{r}\frac{\partial}{\partial r}(r\tau_{rz}) + \frac{\partial \tau_{zz}}{\partial z}\right\} + (1-\beta)\left[\varepsilon^4 \frac{1}{r}\frac{\partial}{\partial r}\left(r\frac{\partial v_z}{\partial r}\right) + \varepsilon^2 \frac{\partial^2 v_z}{\partial z^2}\right] = 0, \tag{9}$$

$$\frac{1}{r}\frac{\partial}{\partial r}(rv_r) + \frac{1}{r}\frac{\partial v_\theta}{\partial \theta} + \frac{\partial v_z}{\partial z} = 0, \tag{10}$$

$$De\left(\frac{\partial \tau_{zz}}{\partial t} + v_r\frac{\partial \tau_{zz}}{\partial r} + v_z\frac{\partial \tau_{zz}}{\partial z} - 2\left\{\frac{\partial v_z}{\partial r}\tau_{rz} + \frac{\partial v_z}{\partial z}\tau_{zz}\right\}\right) + \tau_{zz} = 2\beta\frac{\partial v_z}{\partial z}, \tag{11}$$

$$De\left(\frac{\partial \tau_{\theta z}}{\partial t} + v_r\frac{\partial \tau_{\theta z}}{\partial r} + v_z\frac{\partial \tau_{\theta z}}{\partial z} - r\frac{\partial}{\partial r}\left(\frac{v_\theta}{r}\right)\tau_{rz} - \left\{\frac{v_r}{r} + \frac{\partial v_z}{\partial z}\right\}\tau_{\theta z} - \frac{\partial v_\theta}{\partial z}\tau_{zz} - \frac{\partial v_z}{\partial r}\tau_{r\theta}\right) + \tau_{\theta z} = \beta\frac{\partial v_\theta}{\partial z}, \tag{12}$$

$$De\left(\frac{\partial \tau_{rz}}{\partial t} + v_r\frac{\partial \tau_{rz}}{\partial r} + v_z\frac{\partial \tau_{rz}}{\partial z} - \frac{\partial v_z}{\partial r}\tau_{rr} - \left\{\frac{\partial v_r}{\partial r} + \frac{\partial v_z}{\partial z}\right\}\tau_{rz} - \frac{\partial v_r}{\partial z}\tau_{zz}\right) + \tau_{rz} = \beta\left(\frac{\partial v_r}{\partial z} + \varepsilon^2\frac{\partial v_z}{\partial r}\right), \tag{13}$$

$$De\left(\frac{\partial \tau_{r\theta}}{\partial t} + v_r\frac{\partial \tau_{r\theta}}{\partial r} + v_z\frac{\partial \tau_{r\theta}}{\partial z} + \left(\frac{v_\theta}{r} - \frac{\partial v_\theta}{\partial r}\right)\tau_{rr} - \left\{\frac{\partial v_r}{\partial r} + \frac{v_r}{r}\right\}\tau_{r\theta} - \frac{\partial v_\theta}{\partial z}\tau_{rz} - \frac{\partial v_r}{\partial z}\tau_{\theta z}\right) + \tau_{r\theta} = \varepsilon^2\beta r\frac{\partial}{\partial r}\left(\frac{v_\theta}{r}\right), \tag{14}$$

$$De\left(\frac{\partial \tau_{\theta\theta}}{\partial t} + v_r\frac{\partial \tau_{\theta\theta}}{\partial r} + v_z\frac{\partial \tau_{\theta\theta}}{\partial z} + 2\left(\frac{v_\theta}{r} - \frac{\partial v_\theta}{\partial r}\right)\tau_{r\theta} - 2\frac{v_r}{r}\tau_{\theta\theta} - 2\frac{\partial v_\theta}{\partial z}\tau_{\theta z}\right) + \tau_{\theta\theta} = 2\varepsilon^2\beta\frac{v_r}{r}, \tag{15}$$

$$De\left(\frac{\partial \tau_{rr}}{\partial t} + v_r\frac{\partial \tau_{rr}}{\partial r} + v_z\frac{\partial \tau_{rr}}{\partial z} - 2\left\{\frac{\partial v_r}{\partial r}\tau_{rr} + \frac{\partial v_r}{\partial z}\tau_{rz}\right\}\right) + \tau_{rr} = 2\varepsilon^2\beta\frac{\partial v_r}{\partial r}. \tag{16}$$

For the Oldroyd-B model, the base torsional flow is given by

$$\left.\begin{aligned} &v_r = v_z = 0, \quad v_\theta = rz, \quad P = P_{const} - De\beta r^2, \\ &\tau_{r\theta} = \tau_{rz} = \tau_{rr} = \tau_{zz} = 0, \quad \tau_{\theta z} = \beta r, \quad \tau_{\theta\theta} = 2De\beta r^2. \end{aligned}\right\} \tag{17}$$

### 3.1. *Newtonian case*

Any stability analysis of these viscoelastic solutions relies on the uniqueness of the Newtonian solution. Viscometric measurements using the parallel plate rheometer rely on the fact that the torsional flow solution is valid, which is true only when inertia

is negligible. Hence, in determining the uniqueness of the Newtonian solution we need only consider Stokes flow. The uniqueness of the Newtonian solution becomes important when a stability analysis is conducted on the viscoelastic base solution. If another Newtonian solution exists, its functional form must be excluded from general functional form assumed for the disturbances. The Newtonian solution may also be a reasonable physical solution itself, and possibly the cause of the observed disturbances. The governing Stokes equations in the absence of non-conservative body forces can then be written in cylindrical polar coordinates as

$$-\frac{\partial P}{\partial r}+\varepsilon^2\left\{\frac{\partial}{\partial r}\left[\frac{1}{r}\frac{\partial}{\partial r}(rv_r)\right]+\frac{1}{r^2}\frac{\partial^2 v_r}{\partial\theta^2}-\frac{2}{r^2}\frac{\partial v_\theta}{\partial\theta}\right\}+\frac{\partial^2 v_r}{\partial z^2}=0, \tag{18}$$

$$-\frac{1}{r}\frac{\partial P}{\partial\theta}+\varepsilon^2\left\{\frac{\partial}{\partial r}\left[\frac{1}{r}\frac{\partial}{\partial r}(rv_\theta)\right]+\frac{1}{r^2}\frac{\partial^2 v_\theta}{\partial\theta^2}+\frac{2}{r^2}\frac{\partial v_r}{\partial\theta}\right\}+\frac{\partial^2 v_\theta}{\partial z^2}=0, \tag{19}$$

$$-\frac{\partial P}{\partial z}+\varepsilon^4\left\{\frac{1}{r}\frac{\partial}{\partial r}\left(r\frac{\partial v_z}{\partial r}\right)+\frac{1}{r^2}\frac{\partial^2 v_z}{\partial\theta^2}\right\}+\varepsilon^2\frac{\partial^2 v_z}{\partial z^2}=0. \tag{20}$$

We must also apply the continuity equation, given by (10).

3.1.1. *Non-uniqueness in unbounded flow* ($\varepsilon = 1$)

The uniqueness proofs of Ladyzhenskaya (1969) (which date back to Helmholtz) and others for steady Stokes flow in a domain that is unbounded in some direction require that $\boldsymbol{v} \to \mathbf{0}$ in some sense as $r \to \infty$, usually as $O\left(r^{-1}\right)$. There is no such requirement in this geometry, so the existence of eigenfunctions is a possibility. Axisymmetric eigenfunctions exist, but they involve modified Bessel functions of the first kind ($I_n(r)$), which behave exponentially as $r \to \infty$, an unreasonable demand on the fluid body. For a more physically realistic response we look for a similarity solution of the von Kármán form (von Kármán 1921), and introduce the azimuthal coordinates in a Fourier-type expansion:

$$\left.\begin{aligned}
v_r &= r\left\{u(z)+\sum_{n=0}^{\infty}U_1(z)\cos(n\theta)+U_2(z)\sin(n\theta)\right\},\\
v_\theta &= r\left\{v(z)+\sum_{n=0}^{\infty}V_1(z)\cos(n\theta)+V_2(z)\sin(n\theta)\right\},\\
v_z &= \left\{w(z)+\sum_{n=0}^{\infty}W_1(z)\cos(n\theta)+W_2(z)\sin(n\theta)\right\},\\
P &= P_0(z)+r^2P_2(z)+\sum_{n=0}^{\infty}\left(P_0^c(z)+r^2P_2^c(z)\right)\cos(n\theta)\\
&\qquad +\sum_{n=0}^{\infty}\left(P_0^s(z)+r^2P_2^s(z)\right)\sin(n\theta),
\end{aligned}\right\} \tag{21}$$

Continuity, combined with compatibility in the functional form required by the momentum equations gives $u = -\frac{1}{2}w'$, $U_2 = V_1$, $U_1 = -V_2$, $W_1 = W_2 = P_0^c = P_0^s = 0$, $n = 2$. The Stokes flow solution then becomes

$$\left.\begin{aligned} v_r &= r\left\{P_2^c(z^2-z)\cos 2\theta - P_2^s(z-z^2)\sin 2\theta\right\},\\ v_\theta &= r\left\{z - P_2^c(z^2-z)\sin 2\theta - P_2^s(z-z^2)\cos 2\theta\right\},\\ v_z &= 0,\\ P &= \left\{C + r^2\left[P_2^c\cos 2\theta + P_2^s\sin 2\theta\right]\right\}, \end{aligned}\right\} \tag{22}$$

where $C$ is constant, and $P_2^c$, $P_2^s$ are the amplitudes of the eigenfunctions. To visualize the planar motion, we introduce a stream function

$$v_r = -\frac{1}{r}\frac{\partial\psi}{\partial\theta}, \quad v_\theta = \frac{\partial\psi}{\partial r}.$$

In Cartesian coordinates $(x, y)$, the stream function becomes

$$\psi = \frac{z}{2}\left[\left(1 - P_2^s(1-z)\right)x^2 + P_2^c(1-z)xy + \left(1 + P_2^s(1-z)\right)y^2\right].$$

This is a quadratic form with discriminant

$$\Delta = (1-z)^2\left[\left(P_2^c\right)^2 + 4\left(P_2^s\right)^2 - \frac{4}{(1-z)^2}\right].$$

The streamlines in the $(r,\theta)$-plane are elliptical when $\frac{1}{4}\left(P_2^c\right)^2 + \left(P_2^s\right)^2 \leqslant 1$, and hyperbolae otherwise. It is interesting to note that the functional form in (21) with the functions of $z$ replaced by functions of $z$ and $t$ also reduces the fully time-dependent three-dimensional Navier–Stokes equations by two spatial dimensions and results in a closed system in $v, w, U = U_1, V = V_1$, and $P$. With the notation $\partial f/\partial t = \dot{f}, \partial f/\partial z = f'$,

$$\left.\begin{aligned} Re\left\{-\tfrac{1}{2}\dot{w}' + \tfrac{1}{4}w'^2 - v^2 - \tfrac{1}{2}ww'' + \tfrac{1}{4}\left(U^2+V^2\right)\right\} &= -\tfrac{1}{2}w''' - 2P_2(t),\\ Re\left\{\dot{v} - w'v + wv'\right\} &= v'',\\ Re\left\{\dot{w} + ww'\right\} &= w'' - P_0',\\ Re\left\{\dot{U} - w'U + wU'\right\} &= U'' - 4P_2^c(t),\\ Re\left\{\dot{V} - w'V + wV'\right\} &= V'' + 4P_2^s(t). \end{aligned}\right\} \tag{23}$$

### 3.1.2. *Uniqueness in bounded flow*

The uniqueness proof of the bounded torsional flow can be constructed along the lines of the arguments given in Ladyzhenskaya (1969). Essentially, the dissipation due to the difference between two different (postulated) Stokes solutions is calculated, and is shown to be nil due to the form of the boundary conditions on the upper and lower plates, and the bounding surface at $r = R$. This then leads to a unique solution in this geometry. This is also true in the case of a real free surface at $r = R$, since the boundary conditions are of a similar form.

The situation with a small amount of inertia is quite different. Olagunju (1994) conducted a perturbation analysis of the coaxial disc flow of the Oldroyd-B fluid with inertia. He was able to conclude that a secondary inertial flow existed for all $De$, which became unstable at the critical value

$$De_c = \frac{\pi\sqrt{2}}{[\beta(9+2\beta)]^{1/2}}.$$

Since we are considering purely elastic disturbances to the base flow, we neglect inertia, and the torsional flow solution is valid for all $De$.

## 4. Linear stability analysis

In order to examine the stability of (17), we assume disturbances of the form

$$\left.\begin{aligned} \boldsymbol{v} &= \boldsymbol{v}_o + \delta \mathrm{Re}\left[e^{(\sigma/De)t}\,\boldsymbol{u}(r,z)\right], \\ \tau &= \tau_o + \delta \mathrm{Re}\left[e^{(\sigma/De)t}\,\boldsymbol{\sigma}(r,z)\right], \\ P &= P_o + \delta \mathrm{Re}\left[e^{(\sigma/De)t} p(r,z)\right], \end{aligned}\right\} \tag{24}$$

where $\mathrm{Re}[\cdot]$ represents the real part, and $\boldsymbol{v}_o$, $\tau_o$, and $P_o$ are the base solution.

We can now apply the conditional stability theorem (see, for example, Iooss & Joseph 1980), which states that in order to determine the stability of a solution it is sufficient to study the linearized equations for the perturbed flow about that point, provided that the disturbances are small. This is accomplished by making $\delta$ a small parameter and then linearizing with respect to this variable. The growth rate $\sigma$ determines the stability of the base solution at any particular values of the Deborah number $De$, the retardation parameter $\beta$, and the aspect ratio $\varepsilon$. If $\mathrm{Re}(\sigma) < 0$, the base solution is stable, $\mathrm{Re}(\sigma) > 0$ implies the solution is linearly unstable in this region of $(De, \varepsilon, \beta)$-space, and $\mathrm{Re}(\sigma) = 0$ gives the so called neutral stability curve in the $(De, \varepsilon)$- or $(De, \beta)$-plane.

Substitution of (24) into the constitutive equations yields the perturbed stress field as a function of the perturbed velocities,

$$\sigma_{zz} = \frac{2\beta}{1+\sigma}\frac{\partial u_z}{\partial z}, \tag{25}$$

$$\sigma_{\theta z} = \frac{\beta}{1+\sigma}\frac{\partial u_\theta}{\partial z} + \frac{De\beta r(3+\sigma)}{(1+\sigma)^2}\frac{\partial u_z}{\partial z}, \tag{26}$$

$$\sigma_{rz} = \frac{\beta}{1+\sigma}\left(\frac{\partial u_r}{\partial z} + \varepsilon^2\frac{\partial u_z}{\partial r}\right), \tag{27}$$

$$\sigma_{rr} = \frac{2\varepsilon^2\beta}{1+\sigma}\frac{\partial u_r}{\partial r}, \tag{28}$$

$$\sigma_{r\theta} = \frac{\varepsilon^2\beta}{1+\sigma} r\frac{\partial}{\partial r}\left(\frac{u_\theta}{r}\right) + \frac{De\beta}{(1+\sigma)^2} r\left[(2+\sigma)\frac{\partial u_r}{\partial z} + \varepsilon^2\frac{\partial u_z}{\partial r}\right], \tag{29}$$

$$\sigma_{\theta\theta} = \frac{2De\beta}{(1+\sigma)^3} r\left[(1+\sigma)(2+\sigma)\frac{\partial u_\theta}{\partial z} + (3+\sigma)\,Der\frac{\partial u_z}{\partial z}\right] + \frac{2\varepsilon^2\beta}{1+\sigma}\frac{u_r}{r}. \tag{30}$$

These stresses may then be substituted into the momentum equations to obtain four equations for the perturbed velocity and pressure fields. The pressure term is eliminated, and a stream function introduced so that continuity is identically satisfied,

$$u_r = -\frac{1}{r}\frac{\partial\varphi}{\partial z}, \quad u_z = \frac{1}{r}\frac{\partial\varphi}{\partial r}. \tag{31}$$

The final two governing equations are eventually obtained:

$$(1+\sigma)[1+\sigma(1-\beta)]\left\{\varepsilon^2\frac{\partial}{\partial r}\left(\frac{1}{r}\frac{\partial}{\partial r}(ru_\theta)\right) + \frac{\partial^2 u_\theta}{\partial z^2}\right\}$$
$$+ De\beta\left\{\frac{\partial^3\varphi}{\partial z^2\partial r} - \frac{2(2+\sigma)}{r}\frac{\partial^2\varphi}{\partial z^2} + \varepsilon^2\frac{\partial}{\partial r}\left(\frac{1}{r}\frac{\partial}{\partial r}\left(r\frac{\partial\varphi}{\partial r}\right)\right)\right\} = 0, \tag{32}$$

$$2De\beta(1+\sigma)(2+\sigma)\frac{\partial^2 u_\theta}{\partial z^2}+2De^2\beta(3+\sigma)\frac{\partial^3\varphi}{\partial z^2\partial r}+(1+\sigma)^2[1+\sigma(1-\beta)]$$
$$\times\left\{\frac{1}{r}\frac{\partial^4\varphi}{\partial z^4}+2\varepsilon^2\frac{\partial}{\partial r}\left(\frac{1}{r}\frac{\partial^3\varphi}{\partial z^2\partial r}\right)+\varepsilon^4\frac{\partial}{\partial r}\left(\frac{1}{r}\frac{\partial}{\partial r}\left(r\frac{\partial}{\partial r}\left(\frac{1}{r}\frac{\partial\varphi}{\partial r}\right)\right)\right)\right\}=0. \quad (33)$$

## 5. Numerical solution

The orders of the various derivatives in these equations imply that there must be six boundary conditions in both the radial and axial directions to uniquely define the eigenvalue problem.

The boundary conditions at $r = 0$ are introduced through symmetry arguments. Expressed in terms of the stream function, the stress and velocity boundary conditions at $r = 0, 1$ become

$$\frac{1}{r}\frac{\partial\varphi}{\partial z}=\frac{\partial}{\partial r}\left(\frac{1}{r}\frac{\partial\varphi}{\partial r}\right)=r\frac{\partial}{\partial r}\left(\frac{u_\theta}{r}\right)=0.$$

A mixed Tau–Galerkin procedure was used to solve the equations, utilizing a Fourier series in the axial direction owing to the symmetry of the boundary conditions at $z = 0$ and 1. In the radial direction, a Chebyshev series was chosen, owing to its minimax properties, and its ability to resolve the solution inside a boundary layer (see Gottleib and Orszag 1977).

There also exists the possibility of using a single-domain or multi-domain approach in the discretization of the region. It has been shown (e.g. Peyret 1989), for a Chebyshev spectral method, that a single-domain approach is best for a function which exhibits large variation at $r = \pm 1$, while a multi-domain approach is best for a function with a large variation at $r = 0$.

Making the substitution $r = \frac{1}{2}(x + 1)$, provides the best resolution at both boundaries, owing to the clustering of the zeros of the Chebyshev polynomial at $x = \pm 1$, and the results show that the region of greatest variation in dependent variables is near the outer bounding wall. Hence, a single-domain approach is preferred.

Owing to the symmetry of the geometry, we may assume that $u_r$ and $u_\theta$ are odd functions of $r$, while $u_z$ (and hence $\varphi$) is even in $r$. We can now extend the radial domain to $-1 \leqslant r \leqslant 1$, so that first-kind Chebyshev polynomials can be used in the spectral approximation. This also simplifies the implementation of the singular boundary conditions at the centreline, since they are automatically satisfied by the trial functions.

Following the work of Zebib (1984), the highest-order derivatives of the dependent variables in the governing equations are expanded as series of orthonormal functions:

$$\frac{\partial^4 u_\theta}{\partial r^2\partial z^2}=\sum_{i=0}^{\infty}\sum_{j=0}^{\infty}\alpha_{ij}T_i(r)\cos(j\pi z), \quad (34)$$

$$\frac{\partial^8\varphi}{\partial r^4\partial z^4}=\sum_{i=0}^{\infty}\sum_{j=0}^{\infty}\beta_{ij}T_i(r)\cos(j\pi z); \quad (35)$$

$T_n(r)$ is a Chebyshev polynomial of the first kind, orthonormalized so that $T_0(r) = \pi^{-1/2}$, $T_1(r) = (2\pi)^{1/2}r$, $T_2(r) = (2\pi)^{1/2}(2r^2 - 1)$, $T_{n+1}(r) = 2rT_n(r) - T_{n-1}(r)$, $n > 2$.

These series are then integrated, and the constants of integration determined by the boundary conditions. Once the trial functions are determined, we make the

substitution $x = 2r - 1$, and consider only the region $[0, 1]$ in $r$ or $[-1, 1]$ in $x$. This substitution improves the resolution near $r = 0$ and 1, and greatly increases the rate of convergence of the spectral approximation. The Galerkin trial functions then become

$$u_\theta = \sum_{n=1}^{\infty} \sum_{i=1}^{n} a_{\left(\sum_{k=0}^{n-1} k+i-1\right)} \Lambda_i(x) \Pi_{n-i+1}(z), \tag{36}$$

$$\varphi = \sum_{n=1}^{\infty} \sum_{i=1}^{n} b_{\left(\sum_{k=0}^{n-1} k+i-1\right)} \Psi_i(x) \Phi_{n-i+1}(z), \tag{37}$$

where $\Lambda$, $\Pi$, $\Psi$, and $\Phi$ satisfy all of the imposed boundary conditions.

Consider (32)–(33) as being in the form $\Im_1(u_\theta, \varphi; De, \sigma, \beta, \varepsilon) = 0$, $\Im_2(u_\theta, \varphi; De, \sigma, \beta, \varepsilon) = 0$, respectively, where $\Im_1$ and $\Im_2$ are linear partial differential operators. Also, let $u_{\theta N}$ and $\varphi_N$ be the $N$th partial sums of (36) and (37). We can now introduce the Petrov–Galerkin scheme by forming the residuals of (32) and (33), and taking an appropriate inner product in the usual manner, i.e.

$$\left.\begin{aligned} &\langle \Im_1(u_{\theta N}, \varphi_N), u_{\theta mk} \rangle = 0, \quad u_{\theta mk} = \Lambda_k \Pi_{m-k+1}, \\ &\langle \Im_2(u_{\theta N}, \varphi_N), \varphi_{mk} \rangle = 0, \quad \varphi_{mk} = \Psi_k \Phi_{m-k+1}, \quad m = 1, .., N, \ k = 1, .., m, \\ &\text{with} \\ &\langle u(x,z), v(x,z) \rangle = \int\int_S w(x) u(x,z) v(x,z) \, \mathrm{d}S = \int_0^1 \int_{-1}^1 \frac{1}{(1-x^2)^{1/2}} uv \, \mathrm{d}x \mathrm{d}z. \end{aligned}\right\} \tag{38}$$

### 5.1. *The matrix eigenvalue problem*

Substitution of the spectral approximations into (38) yields an algebraic eigenvalue problem of the form

$$\left[\sigma^3 \boldsymbol{B}_3(De, \beta, \varepsilon) + \sigma^2 \boldsymbol{B}_2(De, \beta, \varepsilon) + \sigma \boldsymbol{B}_1(De, \beta, \varepsilon) + \boldsymbol{A}(De, \beta, \varepsilon)\right] \boldsymbol{v} = 0, \tag{39}$$

known as a cubic eigenvalue problem, where $\boldsymbol{A}$, $\boldsymbol{B}_1$, $\boldsymbol{B}_2$, $\boldsymbol{B}_3$ are all square matrices of size $N(N+1) = N_T$. For each $De$ there will be $3N_T$ eigenvalues $\sigma$ with corresponding eigenvectors $\boldsymbol{v}$. The eigenvector is simply the vector of the unknown coefficients of $u_{\theta N}$ and $\varphi_N$, i.e.

$$\boldsymbol{v} = \left(a_0, a_1, .., a_{N_T/2-1}, b_0, b_1, .., b_{N_T/2-1}\right)^T. \tag{40}$$

In order to examine the linear stability of the base solution (17) we must determine the critical Deborah number ($De_c$) at which the eigenvalue of largest real part crosses the imaginary axis. Let

$$\lambda(\boldsymbol{A}, \boldsymbol{B}_1, \boldsymbol{B}_2, \boldsymbol{B}_3) = \left\{\sigma : \det\left(\sigma^3 \boldsymbol{B}_3 + \sigma^2 \boldsymbol{B}_2 + \sigma \boldsymbol{B}_1 + \boldsymbol{A}\right) = 0\right\}, \tag{41}$$

then the base solution will be linearly stable if $\forall(\sigma \in \lambda(\boldsymbol{A}, \boldsymbol{B}_1, \boldsymbol{B}_2, \boldsymbol{B}_3))$, $\mathrm{Re}(\sigma) < 0$, and unstable if $\exists(\sigma \in \lambda(\boldsymbol{A}, \boldsymbol{B}_1, \boldsymbol{B}_2, \boldsymbol{B}_3))$, $\mathrm{Re}(\sigma) > 0$. Neutral stability will occur at $De_c$ when the eigenvalue with largest real part, $\sigma_c$ is such that $\mathrm{Re}(\sigma_c) = 0$. In this case the critical eigenvalue will have the form $\sigma_c = \sigma_r \pm i\sigma_i$, with $\sigma_r = 0$. As a result, there will be two time-periodic critical eigenfunctions.

Three solution methods are employed in determining the eigenvalues of (39). The first, and most direct, involves treating $\wp(\sigma, De) = \det\left(\sigma^3 \boldsymbol{B}_3 + \sigma^2 \boldsymbol{B}_2 + \sigma \boldsymbol{B}_1 + \boldsymbol{A}\right) = 0$ as a nonlinear equation in $\sigma$. The problem can then be solved by Muller's method for

the complex solutions. This allows for some simplification since there are not strictly $3N_T$ solutions, but only $\frac{5}{2}N_T$ (since $\boldsymbol{B}_3$ is a singular matrix of rank $N_T/2$). There is also the solution $\sigma = -1$, of multiplicity $N_T/2$. Hence we need only solve for $2N_T$ eigenvalues for each $De$. If we solve the system for a particular Deborah number (say $De_0$) we can determine the eigenvalue of largest real part, $\sigma_0$ (in general there will be a complex pair of critical eigenvalues, either of which is suitable, and these can be used to determine the accuracy of each of the numerical schemes). Starting with $\wp(\sigma_0, De_0) = 0$, we can then use some form of tracking scheme (e.g. a homotopy method) to follow $\sigma_0$ as $De_0$ is increased to $De_1$, at which point $\sigma_1$ now lies on the imaginary axis. A simple secant method for $De$ followed by a Muller's method solution for $\sigma$ seems to work if the initial guess is close. There is of course no way of telling if $De_1$ is the critical Deborah number unless we solve the complete problem once again. For a large number of trial functions this method is cumbersome, and Muller's method has difficulty distinguishing between solutions when the eigenvalues are close packed, as in a large system. However, if an estimate of $De_c$ is made with a small number of trial functions, we can use these values as an initial guess for a larger number of trial functions, and obtain a solution quickly since we are only required to find one ordered pair $(\sigma_1, De_1)$. The next two methods are mainly concerned with checking that the solution obtained in this manner is in fact the critical Deborah number.

Equation (39) can be transformed to a generalized eigenvalue problem by letting $\boldsymbol{u} = (\sigma^2\boldsymbol{v}, \sigma\boldsymbol{v}, \boldsymbol{v})^T$. The system then becomes

$$\begin{pmatrix} -\boldsymbol{B}_2 & -\boldsymbol{B}_1 & -\boldsymbol{A} \\ \boldsymbol{I} & 0 & 0 \\ 0 & \boldsymbol{I} & 0 \end{pmatrix} \boldsymbol{u} = \sigma \begin{pmatrix} \boldsymbol{B}_3 & 0 & 0 \\ 0 & \boldsymbol{I} & 0 \\ 0 & 0 & \boldsymbol{I} \end{pmatrix} \boldsymbol{u}, \tag{42}$$

which is in the form of $\Upsilon\boldsymbol{u} = \sigma\,\boldsymbol{\Omega}\,\boldsymbol{u}$, the generalized eigenvalue problem. The solutions can be found using the standard $QZ$ algorithm subject to the consideration that $N_T/2$ of them will be infinite, owing to the rank deficiency of $\boldsymbol{B}_3$. This method works well for medium sized matrices, however it becomes intractable for larger sparse systems.

As the matrices $\Upsilon$ and $\boldsymbol{\Omega}$ become large ( $> 470 \times 470$ or 12 trial functions), a more efficient method is required to solve the large sparse system which results. We use the *enhanced initial vector approach* discussed by Saad (1992). This method is essentially a combination of a Krylov subspace technique and polynomial iteration on the system matrix $\boldsymbol{\Omega}^{-1}\Upsilon$.

Since $\boldsymbol{B}_3$ is singular we must introduce $\mu = \sigma^{-1}$, so that the system becomes

$$\{\boldsymbol{B}_3 + \mu\boldsymbol{B}_2 + \mu^2\boldsymbol{B}_1 + \mu^3\boldsymbol{A}\}\,\boldsymbol{v} = \boldsymbol{0},$$

and with $\boldsymbol{w} = (\mu^2\boldsymbol{v}, \mu\boldsymbol{v}, \boldsymbol{v})^T$, we have the system

$$\begin{pmatrix} -\boldsymbol{B}_1 & -\boldsymbol{B}_2 & -\boldsymbol{B}_3 \\ \boldsymbol{I} & 0 & 0 \\ 0 & \boldsymbol{I} & 0 \end{pmatrix} \boldsymbol{w} = \mu \begin{pmatrix} \boldsymbol{A} & 0 & 0 \\ 0 & \boldsymbol{I} & 0 \\ 0 & 0 & \boldsymbol{I} \end{pmatrix} \boldsymbol{w}.$$

The matrix on the right hand side is now invertible, since $\boldsymbol{A}$ is in general invertible, and we obtain a standard eigenvalue problem

$$\begin{pmatrix} \boldsymbol{A}^{-1} & 0 & 0 \\ 0 & \boldsymbol{I} & 0 \\ 0 & 0 & \boldsymbol{I} \end{pmatrix} \begin{pmatrix} -\boldsymbol{B}_1 & -\boldsymbol{B}_2 & -\boldsymbol{B}_3 \\ \boldsymbol{I} & 0 & 0 \\ 0 & \boldsymbol{I} & 0 \end{pmatrix} \boldsymbol{w} = \boldsymbol{\Sigma}\,\boldsymbol{w} = \mu\,\boldsymbol{w}, \tag{43}$$

where $\boldsymbol{\Sigma}$ is the system matrix.

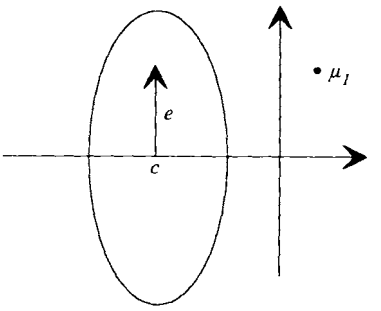


FIGURE 2. Determining outliers of the eigenvalue distribution.

It is important to note that the transformation $\mu = \sigma^{-1}$ preserves the position of the eigenvalues with respect to the half-planes, i.e. if $\mathrm{Re}(\sigma) > 0$ then $\mathrm{Re}(\mu) > 0$, and similarly for the left half-plane. In fact for a general complex number $z = re^{i\theta}$, then the complex mapping $w = z^{-1} = r^{-1}e^{-i\theta}$ results in a vector whose length is $|z|^{-1}$ with argument determined by reflecting $z$ in the real axis.

The infinite eigenvalues encountered in the generalised eigenvalue problem are mapped to 0, giving $N_T/2$ spurious modes at the origin.

In the enhanced initial vector approach we choose an arbitrary starting vector $z_0$, and choose the centre $c$ and focal distance $e$ of an ellipse $E$ in the complex plane. Since $\Sigma$ is a real matrix, the eigenvalues will be placed symmetrically with respect to the real axis, so we choose $c$ to be on the real axis, and $e$ to be either purely real or purely imaginary, see figure 2.

The idea is that if $\mu_1$ is outside the ellipse, then we would like to find a polynomial $p_k(\Sigma)$, of degree $k$ so that, for large $k$, $\mathbf{z}_k = p_k(\Sigma)\, z_0$ approaches a multiple of the eigenvector of $\mu_1$. More precisely, if

$$\mathbf{z}_k = \vartheta_1 \boldsymbol{w}_1 + \sum_{i=2}^{3N_T} \vartheta_i\, p_k(\mu_i)\, \boldsymbol{w}_i,$$

with $p_k(\mu_1) = 1$, and $\wp_k$ the vector space of all polynomials of degree $\leqslant k$, then we wish to find the polynomial which satisfies

$$\min_{p \in \wp_k} \max_{\mu \in E} |p(\mu)|.$$

It turns out that the asymptotically best polynomial ($k \to \infty$) is

$$p_k(\mu) = C_k\left(\frac{\mu - c}{e}\right) \Big/ C_k\left(\frac{\mu_1 - c}{e}\right),$$

where $C_k(\cos\theta) = \cos k\theta$ is the Chebyshev polynomial of the first kind.

In general, the Chebyshev iteration process leads to a vector of the form

$$\mathbf{z}_k = \vartheta_1 \boldsymbol{w}_1 + \vartheta_2 \boldsymbol{w}_2 + \ldots + \vartheta_q \boldsymbol{w}_q + \boldsymbol{\varepsilon},$$

where the eigenvalues $\mu_1, .., \mu_q$ lie outside the ellipse $E$, and $\boldsymbol{\varepsilon}$ is a small vector compared with the others, being the contribution from the eigenvalues inside $E$. To 'purify' $\mathbf{z}_k$ and determine the extreme modes $\mu_1, .., \mu_q$, we use the Arnoldi method, given the fact that the Krylov subspace $K_q \equiv span\{\mathbf{z}_k, \Sigma\mathbf{z}_k, ..., \Sigma^q\mathbf{z}_k\}$ is invariant. Under this condition, the approximate eigenvalues determined by the Arnoldi method will be exactly $\mu_1, .., \mu_q$. It is relatively easy to obtain good estimates for $c$ and $e$ from the use

| $N$ | $N_T$ | $De_c$ | $\sigma_r$ | $\sigma_i$ |
|---|---|---|---|---|
| 4 | 20 | 7.3301 | $5.53 \times 10^{-7}$ | 0.56794 |
| 7 | 56 | 8.0158 | $-1.85 \times 10^{-6}$ | 0.69770 |
| 10 | 110 | 8.0747 | $-8.68 \times 10^{-7}$ | 0.70463 |
| 11 | 132 | 8.0737 | $-2.30 \times 10^{-6}$ | 0.70455 |
| 12 | 156 | 8.0737 | $8.60 \times 10^{-7}$ | 0.70453 |

TABLE 1. Convergence of the linear stability analysis for $\epsilon = 1$ and $\beta = 0.41$

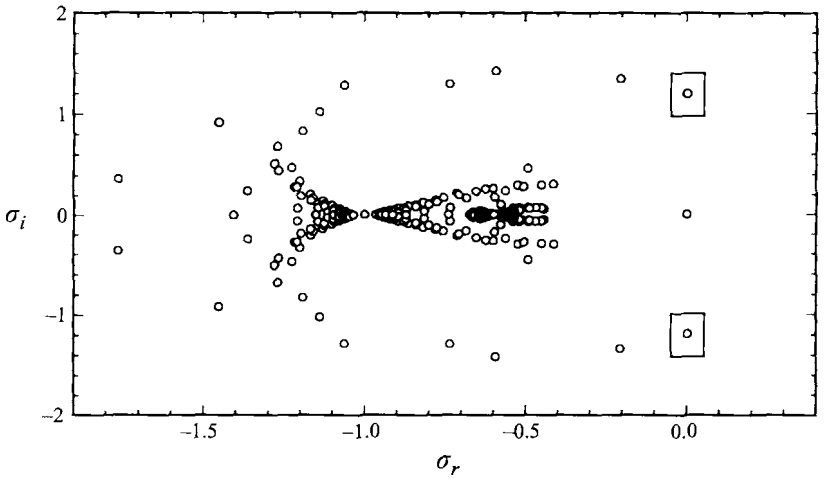


FIGURE 3. Eigenspectrum for $\mu$ obtained by the enhanced initial vector approach; $N = 12$, $\varepsilon = 0.1$ and $\beta = 0.41$, $De = 8.0737$. The critical eigenvalues are boxed.

of a smaller number of trial functions, so that this method is an efficient check that $De_1$ is indeed $De_c$ when we consider a large number of trial functions.

## 6. Convergence results

Owing to the bounding wall at $r = 1$, we cannot take the limit $\varepsilon \to 0$ to obtain the analytic result of Phan-Thien (1983) in order to check the validity of the scheme. Other results (Walsh 1987; Crewthers, Huilgol & Josza 1991; Öztekin & Brown 1993; Byars *et al.* 1994) also use semi-infinite geometry. The perturbation scheme of Olagunju (1994) predicts a different form of instability, so that only qualitative comparison can be made with the existing results.

In table 1 we examine the convergence characteristics of the scheme, for particular values of the material and geometrical parameters. This case required 66 independent trial functions in each of the dependent variables to achieve 5–6 significant figure accuracy in $De_c$. In general convergence is slowed with a decrease in the aspect ratio, though this relationship is not monotonic. Accuracy is also degraded with decreasing $\varepsilon$, as the differing magnitudes of the length scales $h$, $R$ are a feature of stiff boundary value problems in general. At values of $\varepsilon$ of the order 0.1, only 3 to 4 significant figures are possible. Although infinite-order convergence is theoretically possible with the use of this Galerkin scheme, $N$ is restricted by the rapidly increasing condition number of $\Sigma$ with $N$.

Convergence of both Muller's method and Chebyshev iteration is aided by the fact

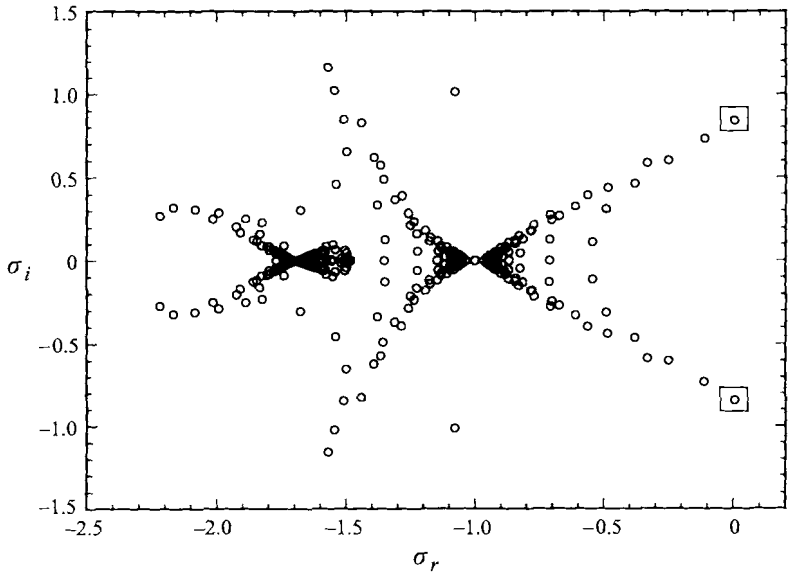


FIGURE 4. Eigenspectrum for $\sigma$ obtained by Muller's method; $N = 12$, $\varepsilon = 0.1$ and $\beta = 0.41$, $De = 8.0737$. The critical eigenvalues are boxed.

that the complex-conjugate pair of critical modes is well separated from the rest of the eigenspectrum, for all values of $N$. Figure 3 shows a typical example for the enhanced initial vector approach while figure 4 shows a typical array used for Muller's method (a total of 312 non-trivial eigenvalues are displayed).

The behaviour of the eigenfunctions is easily determined, and the convergence is illustrated in figure 5 (solid lines represent positive values of the stream function, and dashed lines, negative values). Owing to the axisymmetry we need only consider the $(r, z)$-plane in examining the streamlines $\varphi$.

## 7. Results and discussion

The inclusion of a bounding wall at $r = 1$ leads to significant differences to earlier analyses, both quantitatively, and qualitatively in the critical $De$ and the resulting secondary flow. However, trends such as monotonicity of $De_c$ in $\beta$ are still in agreement with theoretical analyses conducted in the infinite radial geometry (Phan-Thien 1983; McKinley *et al.* 1991; Byars *et al.* 1994; Crewthers *et al.* 1991; etc.). Use of the finite domain requires solving the full two-dimensional problem, since group symmetry reductions or normal mode analysis cannot be applied owing to the extra boundary conditions. It is, however, now possible to determine the effect of a changing aspect ratio on the critical Deborah number and hence the critical shear rate. For this geometry, the rim shear rate $\dot{\gamma} = De/(\lambda\varepsilon)$.

Figure 6 shows the relationship between the critical Deborah number and the retardation parameter, which is a measure of the elasticity of the fluid, for three aspect ratios. Analysis shows that the singularity near $\beta = 0$ scales approximately with the square-root singularity of both the Phan-Thien and Olagunju analyses, shown here by the dotted and dot-dot-dashed lines respectively.

In figure 7 the critical Deborah number is plotted against the aspect ratio. For fluids with an average to high concentration of viscous solvent ($\beta \lesssim 0.5$), there is an almost

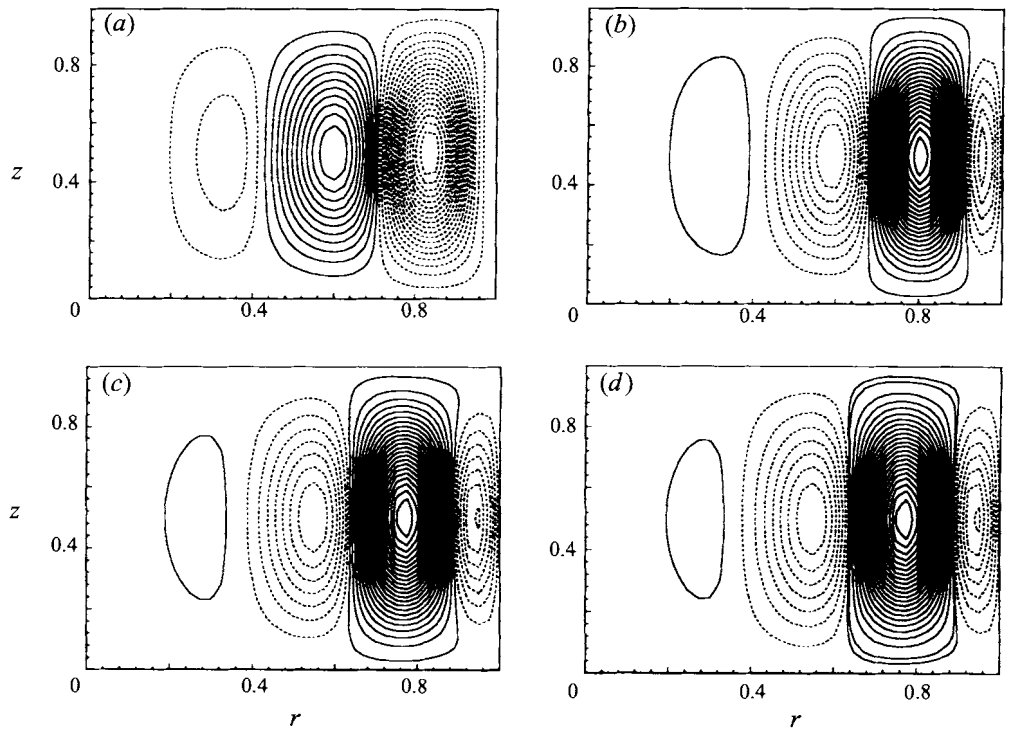


FIGURE 5. Convergence of the disturbance stream function with: (*a*) $N = 6, De = 2.8427$; (*b*) $N = 9, De = 2.8414$; (*c*) $N = 11, De = 2.8434$; (*d*) $N = 12, De = 2.8434$. For all figures $\beta = 0.41, \varepsilon = 0.25$.

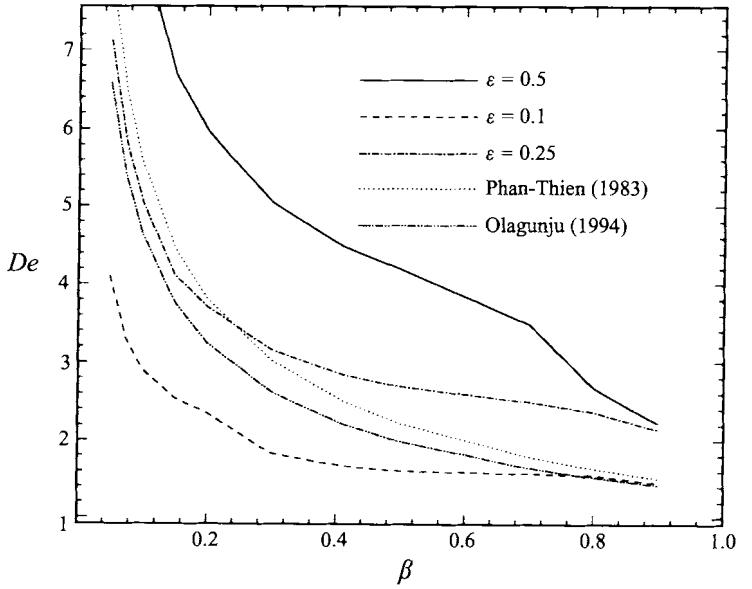


FIGURE 6. The neutral stability curves are plotted in the $(De, \beta)$-plane for several aspect ratios. $\beta = 0$ is the stable Stokes flow, $\beta = 1$ is the Maxwell model.

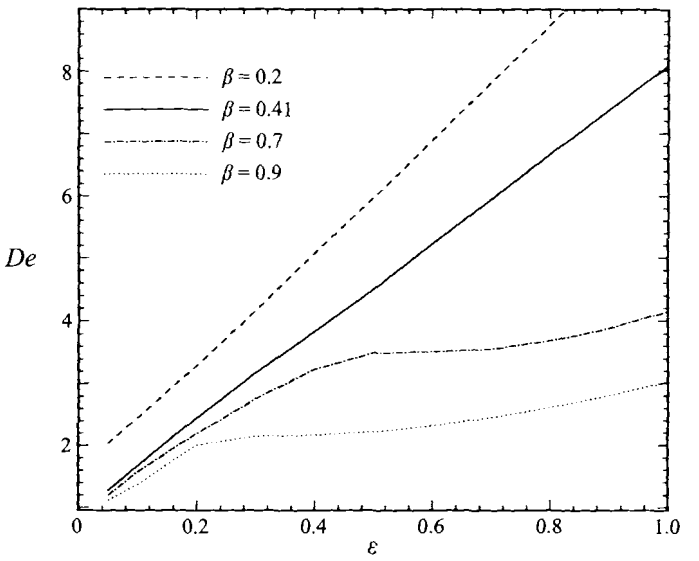


FIGURE 7. Plot of the neutral stability curves in the $(De, \varepsilon)$-plane for a range of $\beta$ values. A linear relationship is apparent for all values of $\beta$ at small aspect ratio.

linear dependency between $De_c$ and $\varepsilon$, while for a lower concentration of solvent this relationship is true for aspect ratios below about 0.2. In fact, the critical Deborah number can be written as $De_c = \varepsilon K_1 + K_2$,where $K_{1,2}$ depend on $\beta$ (for $\beta = 0.41$, which is the relevant value in McKinley *et al.* 1991 and Byars *et al.* 1994, $K_1 = 7.1$ and $K_2 = 1.0$), and the critical dimensionless rim shear rate is $\lambda\dot{\gamma}_c = (K_1 + K_2/\varepsilon)$. This has been observed experimentally by Magda & Larson (1988), and McKinley *et al.* (1994). The critical rim shear rate is inversely proportional to the aspect ratio only when $\varepsilon$ is small. Note that eigenvalues became inaccurate for $\varepsilon \leqslant 0.04$, and they were not plotted.

The nature of the elastic instability becomes apparent when the form of the disturbance stream function is considered. If we assume from the solution to (39) that the stream function is of the form $\varphi = \varphi_r + i\varphi_i$ with $\sigma_c = \pm i\gamma t$, the final disturbance has the form $(\varphi_r \cos\gamma t - \varphi_i \sin\gamma t) \pm i(\varphi_i \cos\gamma t + \varphi_r \sin\gamma t)$. The real and imaginary parts of this function are the two possible forms of the secondary flow. Higher-order analysis is required to determine which of the two is the stable mode. This type of analysis was recently accomplished for the unstable Taylor–Couette flow of the Oldroyd-B fluid by Avgousti & Beris (1994). The two important components of both disturbances are $\varphi_r$ and $\varphi_i$, and these are presented in figures 8 and 9 ($\varphi_r$ is shown in part i and $\varphi_i$ in part ii, the solid lines represent positive values of the stream functions, and dashed lines, negative values). The main difference between $\varphi_r$ and $\varphi_i$ is not readily apparent at small aspect ratios ($\varepsilon < \frac{1}{10}$) and this is due to the fact that the amplitude of the roll cells near $r = 0$ is several orders of magnitude smaller than the amplitude of the roll cells near $r = 1$. This is similar to the type of disturbance predicted by Öztekin & Brown (1993), and observed in Byars *et al.* (1994). In figure 8 we examine the inner region of the discs and find that $\varphi_i$ has roll cells that attenuate towards the centre of the discs near the outer edges. This eigenfunction also has a larger radial wavenumber. We note that for $\varepsilon = \frac{1}{10}$ the $\varphi_r$ has 9 roll cells, while $\varphi_i$ has 10.

In Figure 9(*a*) the streamlines are shown when the aspect ratio is 1. There is a dominant roll cell, surrounded by several smaller cells rotating in the opposite

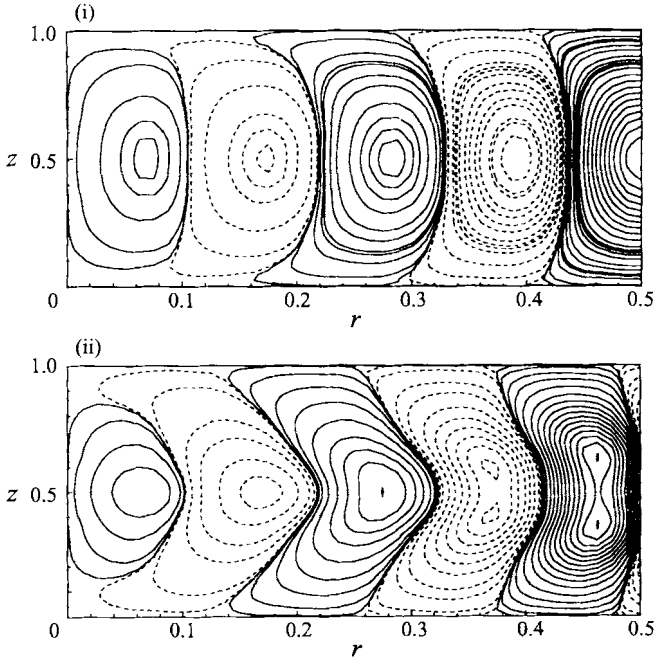


FIGURE 8. The inner region of the flow. The multiple axial roll cells are readily apparent for the geometry with $\varepsilon = 0.1$, $\beta = 0.41$, and $De_c = 1.664$, $\sigma_c = \pm 0.8877\mathrm{i}$.

direction. In figure 9(*b*) the secondary roll cells have disappeared with a decrease in aspect ratio to $\frac{3}{4}$, while a smaller roll cell is developing near $r = 1$ for $\varphi_r$ and near the centreline for $\varphi_i$. This cell is fully developed at $\varepsilon = \frac{1}{2}$ in figure 9(*c*), and the nature of the disturbance for the smaller values of $\varepsilon$ becomes apparent. Roll cells whose diameter scales approximately with the gap width of the discs continue to appear. In the subsequent figures 9(*f*) and 9(*e*) the number of roll cells increase in correspondence with the decreasing aspect ratio.

The form of the disturbance is very similar to that observed by McKinley *et al.* (1991), except that in the present work, the amplitude of the disturbances are large near the outer edge and small near the centreline . In the linear stability region the roll cells would first be seen at the outer edge and then appear to travel inwards, as the amplitude of the inner cells increased exponentially in time. In McKinley *et al.* (1991) cells of large amplitude were observed initially at both the outer edge and at the centreline. A possible reason for this discrepancy is the presence of inertia. Olagunju (1994) conducted a regular perturbation analysis in $\varepsilon$ on the base flow, taking into account the presence of inertia. He found that a secondary flow resulted for all values of $De$ owing to the non-zero Reynolds number. This flow became unstable owing to a blowup in the shear stress at $r = 0$, at a critical value of $De$, and was not due to edge effects. This analysis was certainly valid for the range of Reynolds numbers dealt with in McKinley *et al.* (1991).

Shear thinning of $\Psi_1$ has led to appreciable differences between experimental and theoretical values of $De_c$ for the Oldroyd-B model. McKinley *et al.* (1991) suggested a method of comparing their experimental values with the analysis of Phan-Thien (1983), by allowing $\lambda$, and hence $De$, to be a function of the applied shear rate, i.e., $\lambda = \lambda(\dot{\gamma})$ and $De = De(\dot{\gamma}) = \lambda\Omega$. For the Oldroyd-B model the constant relaxation

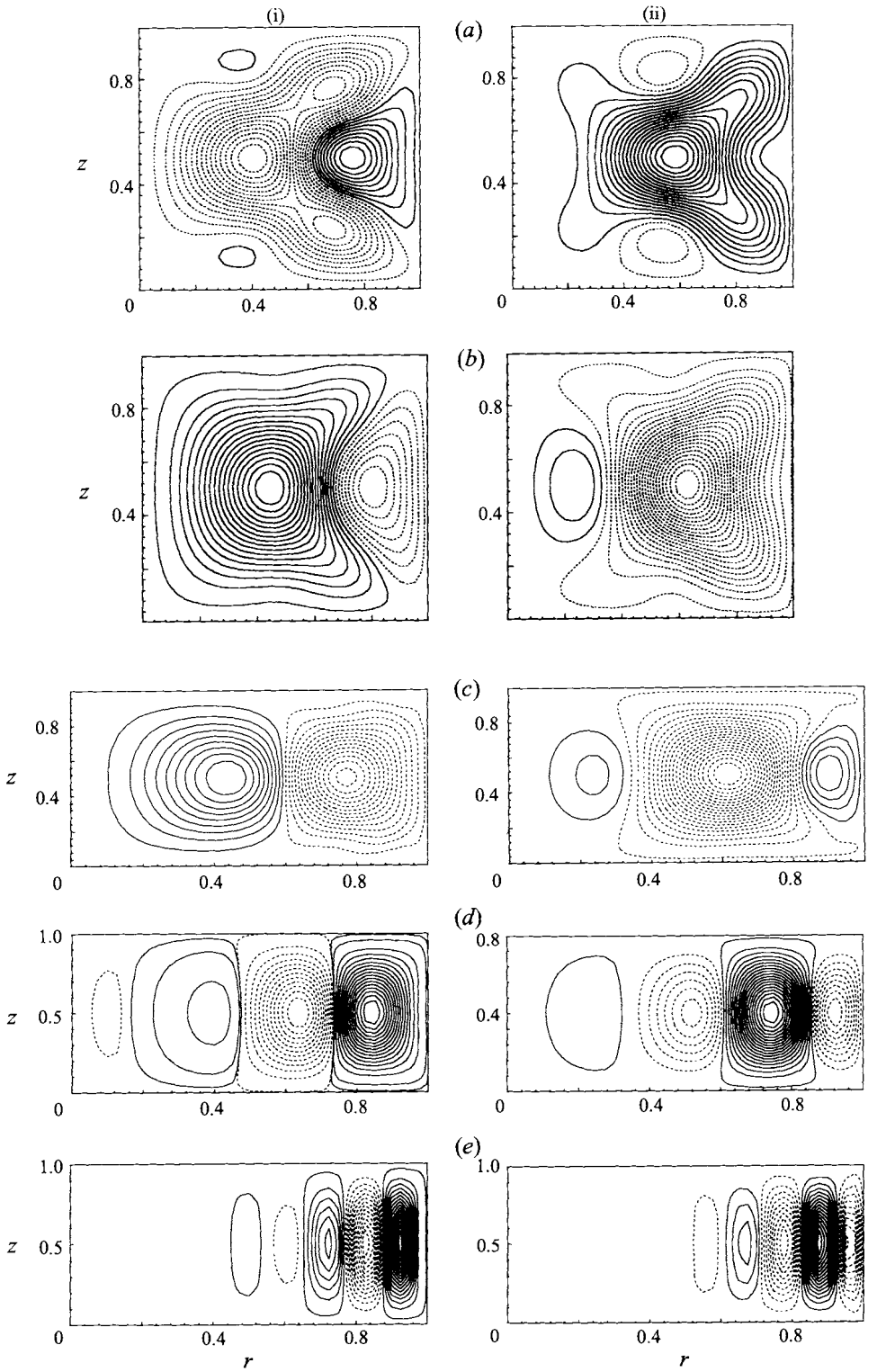


FIGURE 9. Disturbance streamlines at (*a*) $De_c = 7.3262$, $\sigma_c = -1.15 \times 10^{-5} \pm 0.7383\mathrm{i}$, when $\varepsilon = 1$; (*b*) $De_c = 5.747$, $\sigma_c = 6.12 \times 10^{-5} \pm 0.7291\mathrm{i}$, when $\varepsilon = 0.75$; (*c*) $De_c = 4.071$, $\sigma_c = -5.84 \times 10^{-6} \pm 0.7571\mathrm{i}$, when $\varepsilon = 0.5$; (*d*) $De_c = 2.538$, $\sigma_c = 1.47 \times 10^{-4} \pm 0.8156\mathrm{i}$, when $\varepsilon = 0.25$; (*e*) $De_c = 1.664$, $\sigma_c = 6.72 \times 10^{-3} \pm 0.8877\mathrm{i}$, when $\varepsilon = 0.1$,. $\beta = 0.41$.

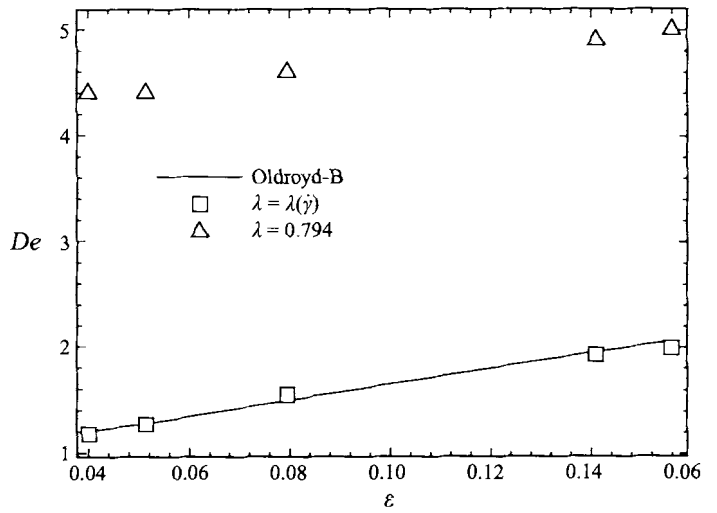


FIGURE 10. Comparison of computed critical modes with experimental values of McKinley *et al.* for constant and adjusted relaxation times. $\beta = 0.41$.

time is determined by the initial value of $\Psi_1$ to be $\lambda_1 = 0.794$. They used a four-mode Bird–DeAguir model to determine $\lambda(\dot{\gamma})$, and plotted stability diagrams of the Weissenberg number $Wi(= \varepsilon De)$ versus $De$, for both models. From these we determined (approximately) the critical Deborah number for several aspect ratios, for both $\lambda_1$ and $\lambda(\dot{\gamma})$. The results are shown in figure 10.

The choice of $\lambda = \lambda(\dot{\gamma})$ results in a significant increase in the correlation between experimental results and the theoretical values obtained with the Oldroyd-B model.

We also note here that the introduction of even a small amount of inertia to the governing equations causes a significant reduction of the critical $De$. For $\beta = 0.41$, Phan-Thien (1983) predicts $De_c = 2.51$, while Olagunju (1994) predicts $De_c = 2.21$, valid for arbitrarily small Reynolds numbers.

## 8. Conclusions

Use of a finite geometry to model parallel plate flow of a Boger fluid has resulted in qualitative and quantitative agreement between theory and experiment, not only in the determination of the critical rotation rate for the onset of elastic instabilities, but also in predicting the form of the resulting disturbance, provided that the relaxation time is estimated from the actual viscometric data at the shear rate where instability occurs. Indeed, if the disturbances, of the non-axisymmetric form $\delta \mathrm{Re}\left[\mathrm{e}^{(\sigma/De)t}\,\boldsymbol{u}(r,z)\mathrm{e}^{im\theta}\right]$, where $m$ is an integer, are allowed to convect with the base flow, then a spiral instability would appear as a wave travelling either from the centre to the outer edge or vice–versa, depending on the sign of the spiral angle. From figure 9(*e*), the amplitude of the disturbances is exceedingly small in the centre region. It would then appear as if the instabilities start beyond a critical radius.

One difficulty of the numerical scheme employed is that convergence is slowed for small $\varepsilon$, and accurate answers were only available for $\varepsilon$ above 0.05. This was due to a rapidly increasing condition number of the system matrix with increasing $N$, and the change in the order of magnitude of the roll cell velocities between the centre of the plates and the outer edge, which was magnified with an increasing number of roll cells, i.e. a reduced value of $\varepsilon$.

Recent evidence, not only in parallel plate flow but also in Taylor–Couette, Taylor–Dean, and in cone-and-plate flows as well, suggests that non-axisymmetric disturbances may be more unstable than those considered here, and that the most unstable mode may alternate between the two types owing to a complex dependence on aspect ratio, and fluid elasticity.

This research is supported by the Australian Research Council (ARC). The support is gratefully acknowledged. We wish to thank all referees for their constructive remarks.

## REFERENCES

AVGOUSTI, M. & BERIS, A. N. 1993 Viscoelastic Taylor-Couette flow: bifurcation analysis in the presence of symmetries. *Proc. R. Soc. Lond.* A **443**, 17–37.

BYARS J. A., ÖZTEKIN, A., BROWN, R. A. & MCKINLEY, G .H. 1994 Spiral instabilities in the flow of highly elastic fluids between rotating parallel discs. *J. Fluid Mech.* **271**, 173–218.

CREWTHERS, I., HUILGOL, R. R. & JOSZA, R. J. 1991 Axisymmetric and nonaxisymmetric flows of a non-Newtonian fluid between coaxial rotating discs. *Phil. Trans. R. Soc. Lond.* A **337**, 467–495.

GOTTLEIB, D. & ORSZAG, S. A. 1977 *Numerical Analysis of Spectral Methods: Theory and Application.* SIAM.

IOOSS, G. & JOSEPH, D. D. 1980 *Elementary Stability and Bifurcation Theory.* Springer.

JACKSON, K. P., WALTERS, K. & WILLIAMS, R. W. 1984 A rheometrical study of Boger fluids. *J. Non-Newtonian Fluid Mech.* **14**, 173–188.

KÁRMÁN, T. VON 1921 Laminare und turbulente Reibung. *Z. Angew. Math. Mech.* **1**, 233–252.

LADYZHENSKAYA, O. A. 1969 *The Mathematical Theory of Viscous Incompressible Flow.* Gordon and Breach.

LARSON, R. G. 1992 Instabilities in viscoelastic flows. *Rheol. Acta* **31**, 213–263.

LARSON, R. G., SHAQFEH, E. S. G. & MULLER, S. J. 1990 A purely elastic instability in Taylor–Couette flow. *J. Fluid Mech.* **218**, 573–600.

MAGDA, J. J. & LARSON, R. G. 1988 A transition occurring in ideal elastic liquids during shear flow. *J. Non-Newtonian Fluid Mech.* **30**, 1–19.

MCKINLEY, G. H., BYARS, J. A., BROWN, R. A. & ARMSTRONG, R. C. 1991 Observations on the elastic instability in cone-and-plate and plate-and-plate flow of a non-Newtonian fluid. *J. Non-Newtonian Fluid Mech.* **40**, 201–229.

OLAGUNJU, D. O. 1994 Effect of free surface and inertia on viscoelastic parallel plate flow. *J. Rheol.* **38**, 151–168.

ÖZTEKIN, A. & BROWN, R. A. 1993 Instability of a viscoelastic fluid between rotating parallel discs: analysis for the Oldroyd-B fluid. *J. Fluid Mech.* **255**, 473–502.

PEYRET, R. 1989 The Chebyshev multidomain approach to stiff problems in fluid Mechanics. In *Proc. ICOSAHOM 1989 Conf. on Spectral and Higher Order Methods for Partial Differential Equations* (ed. C. Canuto & A.Quarteroni).

PHAN-THIEN, N. 1983 Coaxial-disc flow of an Oldroyd-B fluid: exact solution and stability. *J. Non-Newtonian Fluid Mech.* **13**, 325–340.

SAAD, Y. 1992 *Numerical Methods for Large Eigenvalue problems.* Manchester University Press.

WALSH, W. P. 1987 On the flow of a Non-Newtonian fluid between rotating coaxial discs. *Z. Angew. Math. Phys.* **38**, 495–511.

ZEBIB, A. 1984 A Chebyshev method for the solution of boundary value problems. *J. Comput. Phys.* **53**, 443–455.